Improved photoluminescent properties in one-dimensional $LaPO_4:Eu^{3+}$ nanowires

Hongwei Song, Lixin Yu, Shaozhe Lu, Zhongxin Liu, Linmei Yang, and Tie Wang

Key Laboratory of Excited State Physics, Changchun Institute of Optics, Fine Mechanics and Physics, Chinese Academy of Sciences, 16 Eastern South-Lake Road, Changchun 130033, China

Received August 9, 2004

The photoluminescent properties of one-dimensional $LaPO_4$:Eu nanowires were studied in contrast with the corresponding zero-dimensional nanoparticles, micrometer particles, and micrometer rods. The results indicate that in nanowires Eu^{3+} ions occupied two different symmetry sites, unlike in nanoparticles and micrometer particles. Furthermore, the radiative transition rate of $^5D_1-\sum_J {}^7F_J$ or $^5D_0-\sum_J {}^7F_J$ and the internal luminescent quantum efficiency of Eu^{3+} in the nanowires showed obvious improvement over that in the other powders.

OCIS codes: 160.2540, 300.2530.

One-dimensional devices such as nanowires (NWs) and nanotubes have received extensive attention in both fundamental and applied studies.[1–3] They not only can play a crucial role in important future optoelectronic devices,[2,4] data storage,[5] and biochemical and chemical sensors[6] but also can be used to enrich our understanding of basic quantum mechanics.[7] Rare-earth (RE) compounds have been extensively applied to high-performance magnets, luminescent devices, catalysts, and other functional materials. Most of these functions depend strongly on the composition and structure. In the past decade RE-doped zero-dimensional nanoparticles (NPs) have been widely studied because of their potential application in lighting and high-resolution display.[8–10] Recently the preparation of RE-doped one-dimensional devices such as $LaPO_4$:RE (RE = Eu^{3+}, Tb^{3+}) NWs[11] and Y_2O_3:RE nanotubes,[12,13] and the luminescent properties of NPs have also attracted considerable interest. However, until now their luminescent properties did not compare well with those of zero-dimensional and micrometer-sized materials. Micrometer-sized $LaPO_4$ is a well-known host for lanthanide ions. Ce/Tb codoped $LaPO_4$ has been used in fluorescent lamps, CRTs, and plasma display panels. Eu^{3+} ions are sensitive activators for use in the study of local symmetry.[14,15] Recently we successfully prepared $LaPO_4$ NPs and NWs doped with different RE materials (Tb, Ce, Eu).[16] In this Letter we focus on the luminescent properties of $LaPO_4$:Eu to demonstrate the structural and photoluminescent differences between NW and NP as well as the micrometer-sized powders. It is significant to observe that Eu^{3+} in one-dimensional NW has a higher radiative transition rate than that in zero-dimensional NPs and micrometer-sized materials as a result of shape anisotropy.

$LaPO_4$:Eu NPs, NWs, and the corresponding micrometer particles (MPs) and micrometer rods (MRs) were prepared by use of a wet-chemical method originally reported by Meyssamy *et al.*[11] In the synthesis appropriate amounts of La_2O_3 and Eu_2O_3 (1:0.05 mol. ratio) were dissolved into concentrated HNO_3 solution and distilled water was added. Then $(NH_4)_2HPO_4$ solution (0.18 M) was added to the solution. The pH value of the mixed solution was adjusted to 12–13 for NPs and 1–2 for NW. After it was stirred well, the colloid solution was poured into Teflon-lined autoclaves and subsequently heated at 120 °C for 3 h. The obtained suspension was run through a centrifuge and the supernatant was discarded. The resultant precipitation was washed with distilled water and dried at 50 °C. $LaPO_4$:Eu MPs and MRs were prepared by the same method at 150 °C. The practical concentrations of Eu^{3+} ions in a matrix, obtained by use of a plasma spectra method, were 4.15% in NPs, 4.32 mol. % in NW, 4.36 mol. % in MPs, and 4.41 mol. % in MRs. In the measurements the samples were put into a liquid helium cycling system (10–300 K). A 266-nm light generated from a fourth-harmonic generator pumped by a pulsed Nd:YAG laser was used as the excitation source. The spectra and dynamics were recorded by a Spex-1403 spectrometer, a photomultiplier, and a boxcar integrator and processed by a computer.

Figure 1 shows transmission electron micrographs and scanning electron micrographs of $LaPO_4$:Eu powders. As can be seen from the figure, the morphology

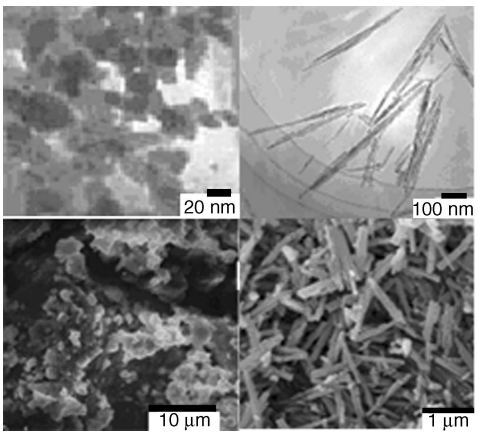

Fig. 1. Top row, transmission electron micrographs of $LaPO_4$:Eu NPs and NWs and (bottom row) scanning electron micrographs of MPs and MRs.

0146-9592/05/050483-03$15.00/0

of the samples differed with the solution pH value in the synthesis process: the colloidal NPs/MPs were basic, and the NW/MRs were acid. The sizes of the $LaPO_4$:Eu NPs ranged from 10 to 20 nm. The diameter of the $LaPO_4$:Eu NW ranged from 10 to 20 nm, and the length had a range of several hundred nanometers. Spherical MPs with a diameter of 1–2 μm were formed in the basic solution at 150 °C, and MRs with a diameter of ~200 nm and a length of 1–2 μm were formed in acid. Figure 2 shows x-ray diffraction patterns of different $LaPO_4$:Eu powders. It can be seen that the crystal structure of all the samples belongs to monoclinic monazite type. The relative intensity of the diffraction peaks in the range 40–55° in the NW decreased compared with the other samples because of shape anisotropy.

The local structure surrounding the Eu^{3+} ions in the different samples was studied and compared next. $LaPO_4$ belongs to the monazite type. In $LaPO_4$ systems, La^{3+} ions occupy the C_1 point group. In Eu^{3+}-doped $LaPO_4$, Eu^{3+} ions substitute for some of the La^{3+} ions. Figure 3 shows high-resolution spectra of different $LaPO_4$:Eu powders. Note that the peaks labeled with stars in Fig. 3 were for the $^5D_1$–$^7F_4$ transitions, which were identified according to time-resolved emission spectra and the energy levels of $LaPO_4$:Eu^{3+}. As is known from Ref. 16, $^5D_0$–$^7F_1$ transitions are hypersensitive to the crystal field. $^7F_1$ in one symmetry site can split into three Stark levels ($2J + 1$). Different sites may generate different groups of levels. In the NPs, three $^5D_0$–$^7F_1$ emission lines appeared (L1–L3). In the NWs, besides the same lines 1–3, three additional lines (4–6) also appeared. The $^5D_0$–$^7F_1$ lines in the MPs are entirely identical to the NPs, indicating that site symmetry in MPs is the same as that in NPs. As in the NWs, lines 1–6 also appeared in the MRs. However, the relative intensity of lines 4–6 in the MRs became weaker than that in the NWs. The results in Fig. 3 indicate that in the NPs and MPs the $^5D_0$–$^7F_1$ transitions came from one crystalline site, A, whereas in the NWs and MRs the $^5D_0$–$^7F_1$ transitions came from the same site (L1–L3), A, and an additional site (L4–L6), B. The relative number of Eu^{3+} ions occupying site B decreased as the powders changed from NW to MRs. In Fig. 3 the Stark lines of the $^5D_0$–$^7F_2$ emissions were not completely identified because they overlapped to some extent. The site-selective excitation experiments further indicate that in the NW the $^5D_0$–$^7F_2$ emissions originated from two different sites, whereas in the NPs they originated from only one site.

For MPs to NPs (20 nm) the surface-to-volume ratio varied greatly, but the site symmetry was the same. In the NW, despite the fact that the surface-to-volume ratio did not decrease from that in the NPs, Eu^{3+} occupied an additional site, B. Apparently the appearance of the additional site was due not to a surface effect but to shape anisotropy. We studied the high-resolution transmission electron micrograph images of $LaPO_4$:Eu NW and observed that the internal atoms were neatly arranged, and the arrangement of the atoms in the fringe along the length direction degenerated. This will lead the crystal field surrounding Eu^{3+} in the fringe to be different from that in the interior, leading to the appearance of the new site B. The crystal degeneration in the fringe of NW is probably related to the sample preparation conditions.

Next the electronic transition processes were studied. Assuming that the nonradiative relaxation of $^5D_1$–$^5D_0$ is a multiphonon process, the lifetime of $^5D_1$ under 266-nm excitation can be expressed as[16]

$$\tau = \frac{1}{W_1 + W_{10}(0)[1 - \exp(-\hbar\omega/kT)]^{-\Delta E_{10}/\hbar\omega}}, \quad (1)$$

where W_1 is the radiative transition rate of $^5D_1$–$\sum_J {}^7F_J$, $W_{10}(0)$ is nonradiative transition rate at 0 K, ΔE_{10} is the energy separation between $^5D_1$ and $^5D_0$, $\hbar\omega$ is the photon energy, k is the Boltzmann constant, and T is the absolute temperature.

Figure 4 shows the dependence of $^5D_1$–$^7F_2$ exponential lifetimes on temperature in different samples. It can be observed that the fluorescence lifetime of

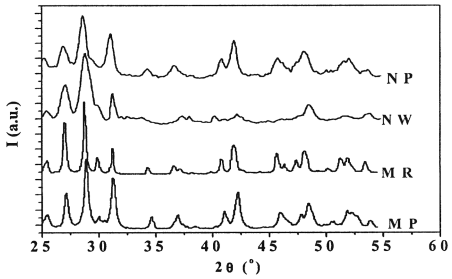

Fig. 2. X-ray diffraction patterns of $LaPO_4$:Eu NPs, NW, MPs, and MRs.

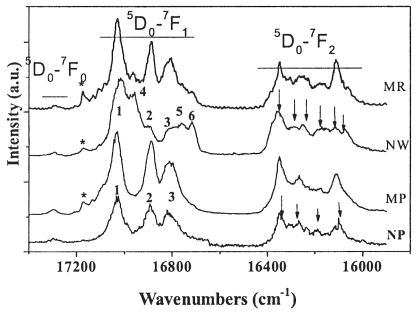

Fig. 3. High-resolution spectra of different $LaPO_4$:Eu powders at 10 K under 266-nm excitation.

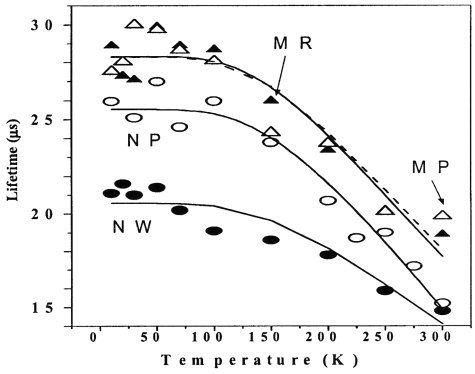

Fig. 4. Dependence of $^5D_1$–$^7F_2$ fluorescence lifetime (at 18,070 cm^{-1}) on temperature in different powders. Shapes, experimental data; solid curves, fitting functions.

$^5D_1-^7F_2$ nearly reversed as a constant below 100 K and decreased rapidly above 100 K for all the samples. In Fig. 4 the experimental data were well fitted with Eq. (1). In the fitting, ΔE_{10} was fixed at 1758 cm^{-1} for different samples, because their energy levels had only a little variation and had no influence on the calculation. We chose $\hbar\omega$ to be 390 cm^{-1} according to the Raman spectrum, which showed that the peak at ~390 cm^{-1} was the strongest vibration mode.

By this fitting process we obtained W_1 and $W_{10}(0)$ for different powders: 14.9 and 24.1 ms^{-1} in NPs, 28.9 and 19.7 ms^{-1} in NW, 17.6 and 17.8 ms^{-1} in MPs, and 16.5 and 18.5 ms^{-1} in MR. The radiative transition rate of $^5D_1-\sum_J {}^7F_J$ in the MPs and the MRs was nearly the same. The radiative transition rate in the NPs had only a little variation compared with the MPs and MRs, whereas that in the NW increased by 63%. In comparison with the MPs and MRs, the nonradiative transition rate of $^5D_1-^5D_0$ in the NPs increased ~25%, and in the NW it increased only a little. The luminescent quantum efficiencies for the $^5D_1$ level at 0 K were thus determined to be 59, 30, 49, and 47% in NW, NPs, MPs, and MRs, respectively. It is obvious that the quantum efficiency of Eu^{3+} in the NW increased from that in the NPs, MPs, and MRs.

The fluorescence lifetime of the $^5D_0-^7F_2$ transition as a function of temperature (10–300 K) in different samples was also measured. As the temperature varied from 10 to 300 K, the $^5D_0$ lifetimes in all samples hardly changed. The lifetime of $^5D_0-^7F_2$ at room temperature (at 16,342 cm^{-1}) was 2.25 ms in the NPs, 1.63 ms in the NW, 2.32 ms in the MPs, and 2.40 ms in the MRs. $^5D_0$ is the lowest excited state, and the energy separation between $^5D_0$ and the nearest downlevel $^7F_6$ is as high as ~12,000 cm^{-1}. In this case nonradiative relaxation processes hardly happen, according to the theory of multiphoton relaxation. Thus we suppose that the radiative transition rate of $^5D_0-\sum_J {}^7F_J$ equals the inverse of the fluorescence decay time. Then, the radiative transition rate of $^5D_0-\sum_J {}^7F_J$ was deduced to be 0.61 ms^{-1} in the NW, 0.44 ms^{-1} in the NPs, 0.43 ms^{-1} in the MPs, and 0.42 ms^{-1} in the MRs. The radiative transition rate of $^5D_0-\sum_J {}^7F_J$ in the NWs also increased greatly compared with that in the other samples.

For RE ions the diameter of the electronic wave function of the f electrons is of the order of 10^{-1} nm, which is much smaller than the particle diameter, indicating the absence of a confinement effect.[16] The radiative fluorescence lifetime is proportional to the reverse of the oscillator strength of the electronic dipole transition f(ED) (Ref. 17); f(ED) is strongly dependent on the crystal field and the electronic–magnetic dipole field surrounding the Eu^{3+} ions. The shape anisotropy will hardly influence the crystal field but will influence the dipole field caused by the excited ion. We suggest that the shape anisotropy affects the ionic dipole field and therefore the photonic density of states and thus the radiative transition rate. In the NPs and NW the nonradiative transition rate increased compared with that in the MPs with different content. This difference can be attributed to a surface effect. On the surface a large number of defects generally exist that act as nonradiative transition channels, increasing the nonradiative transition rates.

In conclusion, the luminescent properties of $LaPO_4$:Eu powders have been studied. The results indicate that Eu^{3+} in NW and MRs occupied an additional site B besides the same site A as was occupied in MPs and NPs. This result was attributed to the degeneration of the crystal field in the fringe region of the wirelike powders. Unlike in NPs, MPs, and MRs, the radiative transition rate of $^5D_1-\sum_J {}^7F_J$ and $^5D_0-\sum_J {}^7F_J$ and the quantum efficiency for $^5D_1$ in the NW was obviously increased as a result of the variation of the electronic–magnetic dipole field caused by shape anisotropy.

The authors are grateful for financial support from the "One Hundred Talents Project" of the Chinese Academy of Sciences and the National Natural Science Foundation of China (grants 10374086 and 10274083).
H. Song's e-mail address is songhw67@sina.com.cn.

References

1. S. Lijima, Nature **354,** 56 (1991).
2. X. F. Daun, Y. Huang, Y. Cui, J. F. Wang, and C. M. Lieber, Nature **409,** 66 (2001).
3. E. C. Dickey, C. A. Crimes, M. K. Jain, K. G. Ong, D. Qian, P. D. Kichambare, R. Andrews, and D. Jacques, Appl. Phys. Lett. **79,** 4022 (2001).
4. H. Kind, H. Yan, M. Law, B. Messer, and P. Yang, Adv. Mater. **14,** 158 (2002).
5. P. M. Ajayan, O. Stephan, P. Redlich, and C. Colliex, Nature **375,** 564 (1995).
6. Y. Cui, Q. Wei, H. Park, and C. M. Lieber, Science **299,** 1874 (2003).
7. D. D. Ma, C. S. Lee, F. C. K. Au, S. Y. Tong, and S. T. Lee, Science **293,** 1289 (2003).
8. D. Matsuura, Appl. Phys. Lett. **81,** 4526 (2002).
9. Z. Wei, L. Sun, C. Liao, and C. Yan, Appl. Phys. Lett. **80,** 1447 (2002).
10. K. Riwotzki, H. Meyssamy, A. Kornowski, and M. Hasse, J. Phys. Chem. **104,** 2824 (2000).
11. H. Meyssamy, K. Riwotzki, A. Kornowski, S. Naused, and M. Haase, Adv. Mater. **11,** 840 (1999).
12. M. Yada, M. Mihara, S. Mouri, and T. Kijima, Adv. Mater. **14,** 309 (2002).
13. C. Wu, W. Qin, G. Qin, D. Zhao, J. Zhang, and S. Huang, Appl. Phys. Lett. **82,** 520 (2003).
14. H. Song, L. Yu, S. Lu, T. Wang, Z. Liu, and L. Yang, Appl. Phys. Lett. **85,** 470 (2004).
15. H. Peng, H. Song, B. Chen, J. Wang, S. Lu, and J. Zhang, Chem. Phys. Lett. **370,** 485 (2003).
16. H. Song, J. Wang, B. Chen, and S. Lu, Chem. Phys. Lett. **376,** 1 (2003).
17. R. S. Meltzer, S. P. Feofilov, B. Tissue, and H. B. Yuan, Phys. Rev. B **60,** 14012 (1999).